EUV spectroscopy of the Venus dayglow with UVIS on Cassini

J.-C. Gérard, B. Hubert, J. Gustin
LPAP, Université de Liège, Belgium

V. I. Shematovich, D. Bisikalo
INASAN, Moscow, Russian Federation

G.R. Gladstone

SWRI, San Antonio, Tx, USA

L.W. Esposito

LASP, University of Colorado, Boulder, Co, USA

Submitted for publication to ICARUS

Revised, August 2010

Corresponding Author:

J.-C. Gérard

Université de Liège
Institut d'Astrophysique et de Géophysique
17, Allée du 6 Août, B5c
B-4000 Liège
Belgium

Tel : +32 (0)4 366 97 75
Fax : +32 (0)4 366 97 11

e-mail : jc.gerard@ulg.ac.be

Abstract

We analyze EUV spatially-resolved dayglow spectra obtained at 0.37 nm resolution by the UVIS instrument during the Cassini flyby of Venus on 24 June 1999, a period of high solar activity level. Emissions from OI, OII, NI, CI and CII and CO have been identified and their disc average intensity has been determined. They are generally somewhat brighter than those determined from the observations made with the HUT spectrograph at a lower activity level, We present the brightness distribution along the foot track of the UVIS slit of the OII 83.4 nm, OI 98.9 nm, Lyman-ß + OI 102.5 nm and NI 120.0 nm multiplets, and the CO C-X and B-X Hopfield-Birge bands. We make a detailed comparison of the intensities of the 834 nm, 989 nm, 120.0 nm multiplets and CO B-X band measured along the slit foot track on the disc with those predicted by an airglow model previously used to analyze Venus and Mars ultraviolet spectra. This model includes the treatment of multiple scattering for the optically thick OI, OII and NI multiplets. It is found that the observed intensity of the OII emission at 83.4 nm is higher than predicted by the model. An increase of the O^+ ion density relative to the densities usually measured by Pioneer Venus brings the observations and the modeled values into better agreement. The intensity of the OI 98.9 nm emission is well predicted by the model if resonance scattering of solar radiation by O atoms is included as a source. The calculated intensity variation of the CO B-X emission along the track of the UVIS slit is in fair agreement with the observations. The calculated brightness of the NI 120 nm multiplet is larger than observed by a factor of ~2-3 if photons from all sources suffer multiple scattering. The difference reduces to 30 – 80% if the photon electron impact and photodissociation of N_2 sources of N atoms are considered as optically thin. Overall, we find that the O, N_2 and CO densities from the empirical VTS3 model provide satisfactory agreement between the calculated and the observed EUV airglow emissions.

Keywords: Keywords: Venus, atmosphere, Ultraviolet observations, aeronomy, radiative transfer

1. Introduction

The first spectra at moderate spectral resolution of the Venus ultraviolet dayglow were obtained using a rocket-borne spectrometer by *Moos et al.* (1969) and *Moos and Rottman* (1971) on 5 December 1967 and 25 January 1971 respectively. However, the spectral range was limited to 120-190 nm and did not include any emission at wavelengths shorter than Ly-α at 121.6 nm. The Mariner 10 spacecraft flew by Venus in February 1974 carrying an objective grating spectrometer with channel electron multipliers at nine fixed wavelengths between 20 and 170 nm (Broadfoot et al., 1974). Strong emissions were detected at the wavelengths of the HeI feature at 58.4 nm, Lyman-α at 121.6 nm, and the OI resonance triplet at 130.4 nm. No measurable signal was obtained in the channels including multiplets belonging to HeII at 30.4nm, NeI at 74 nm or ArI at 86.9 nm. A similar instrument was flown on board the Soviet Venera 11 and 12 spacecraft which flew by Venus on December 25 and 21, 1978 as the sun activity was rising towards solar maximum conditions (Bertaux et al., 1981). In addition to those emissions previously detected from Mariner 10, the Venera spectrometers measured the disc brightness of the HeII multiplet at 30.4 nm and altitude profiles of the Ly-α and HeI 58.4 nm emissions were also reported. The first measurements of the intensity of the OII emission at 83.4 nm were made with Venera 11, giving a maximum intensity of 156 R on the disc. *Stewart and Barth* (1979) obtained a large number of mid-resolution (~1.3 nm) dayglow spectra with the Orbiting UltraViolet Spectrometer (*Stewart,* 1980) on board Pioneer-Venus, but the spectral coverage was limited to wavelengths above 120 nm. The processes leading to excitation of the Venus ultraviolet airglow and its remote sensing were reviewed by *Fox and Bougher* (1991) and *Paxton and Anderson* (1992).

The only complete EUV dayglow spectrum of Venus available so far was analyzed by *Feldman et al.* (2000) who used the Hopkins Ultraviolet Telescope (HUT) instrument on board the Space Shuttle to observe the Venus disc on 13 March 1995, near solar minimum

($F_{10.7}$ index = 82). The HUT spectrum integrated the dayglow emission over the sunlit fraction, estimated as approximately 60% of the disc. The instrument covered the spectral range 82-184 nm at ~0.4 nm resolution and provided brightness of spectral signatures from OI, OII, CI, CII, NI and CO. Feldman et al. reported the disc-averaged brightness of 13 emissions identified within the HUT spectral range and set an upper limit on the brightness of several argon lines.

Recently, Hubert et al. (2010) analyzed FUV spatially-resolved dayglow spectra of Venus in the 111.5- 191.2 nm bandwidth at 0.37 nm resolution, obtained with the Ultraviolet Imaging Spectrograph (UVIS) during the Cassini flyby of Venus in June 1999. They concentrated on the OI 130.4 triplet and 135.6 nm doublet and the CO A-X Fourth Positive (4P) system. They compared the brightness observed along the UVIS foot track of the two OI multiplets with that deduced from an airglow model where the neutral atmospheric densities were taken from the VTS3 empirical atmospheric model by Hedin et al. (1993). Using the EUV solar intensities appropriate to the time of the observation, the intensities they calculated were found to agree with the observed 130.4 nm brightness within ~10% and the OI 135.6 nm brightness was also reasonably well reproduced by the model. They also found that self-absorption of the (0-v”) bands of the CO 4P emission is important and derived a CO vertical column in close agreement with the value provided by the VTS3 model.

In this study, we analyze the spatially resolved EUV dayglow spectra obtained with UVIS during the Cassini flyby of Venus. We determine the average brightness of several relatively bright emissions and discuss the identification of several weaker features. We compare the observed intensities with those derived from the HUT disc spectra obtained during a period of lower solar activity. We also present the variation across the sunlit disc of several emissions and compare the intensities of some of them with the brightness derived from a Venus airglow model.

2. Observations

The Cassini spacecraft flew by Venus on 24 June 1999 to gain gravitational assist on its way to Saturn. Periapsis occurred at 20:30:07 UT when the spacecraft reached an altitude of 602 km. At this period, solar activity was rising, reaching a F10.7 solar index ~214 at Earth distance. The UVIS spectrograph (*Esposito et al.,* 1998) obtained a series of simultaneous FUV and EUV spectra during this swingby. The UVIS line of sight was oriented nearly perpendicular to the Sun-spacecraft line, so that the phase angle remained close to 90°. Fifty-five records of 32s each were obtained along the track, twenty-five of which observed the sunlit disc of Venus. The overall observing time on the sunlit disc is about 13 minutes. The latitude of the UVIS slit footprint on the planet varied from ~24° North to ~15° South. Figure 1 shows the foot track geometry and describes the variation of the solar zenith angle (SZA) and emission angle (the angle between the line of sight and local zenith at the altitude of airglow emission). The SZA varied along the track from 90° at the morning terminator to 0° when the UVIS line of sight reached the sunlit planetary limb. These values and some of the instrumental characteristics are summarized in Table 1.

The total spectral range spanned by UVIS extends from 56.3 to 191.2 nm and is covered by two separate channels. The bandpasses of the EUV and FUV channels are 56.3-118.2 nm and 111.5-191.2 nm, respectively. The two channels have similar resolving power but different channel width, slit width, field of view, optical coatings, diffraction grating rulings and detector photocathodes. The two-dimensional format for the CODACON detectors allows simultaneous spectral and one-dimensional spatial coverage. The UVIS slit image on the detector is composed of 1024 pixels in the dispersion direction and 64 pixels in the spatial direction. The full spectral resolution has been used during the Venus observations, while the spatial direction has been rebinned by 16 pixels, leaving a resolution of 4 pixels along the spatial direction. Each record presented here is the sum of the two central spatial pixels in order to increase the signal/noise ratio. The FUV field of view along the slit is 64 mrad, corresponding to ~450 km projected on the planet surface from an altitude of 7000 km. The spacecraft moved ~500 km during the 32 second integration period of each record. The slit was oriented nearly perpendicular to the ecliptic plane. From the three UVIS slits available (high-resolution, low-resolution and occultation), the high-resolution slit was used for the Venus observations, providing spectra at a resolution of ~0.37 nm FWHM.

3. The UVIS EUV disc spectrum

The UVIS instrument offers the advantages of a wide spectral coverage, high sensitivity, medium spectral resolution, and spatially resolved spectroscopy of the Venus EUV and FUV day airglow emissions. The EUV data have been calibrated following the pre-flight measurements described by Esposito et al., (2004). An empirically derived background noise level of 4.5×10^{-4} counts s^{-1} $pixel^{-1}$ due to the radioisotope thermoelectric generators has been removed and a flat-field correction derived from observations of Spica (Steffl et al., 2004) has been applied. Two contaminating signals also affect the EUV spectra. The first is due to internal scattering of Ly-α, focused beyond the long wavelength end of the EUV detector and estimated to contribute less than 7% of the total signal (Ajello et al., 2005). The second is caused by a small light leak that allows undispersed interplanetary Ly-α to reach the portion of the EUV detector corresponding to wavelengths shorter than 92 nm. The signal associated to this leak smoothly rises from 0.063 count/pixel s at 56 nm to 0.125 count/pixel s at 92 nm and rapidly drops to zero at 102 nm. This background signal has been manually subtracted from the data, but a fairly high noise level is associated with this stray signal.

Consequently, the residual spectrum in this region is quite uncertain and we have not attempted to make any spectral assignment below 93 nm, with the exception of the bright O^+ emission at 83.4 nm. The sensitivity below 90 nm significantly decreases, leading a more noisy signal than at longer wavelengths. This makes it difficult to determine the brightness of weak features in this region, even though features may appear relatively bright when expressed in R/nm.

The count rate has been converted into physical units using the latest calibration routine. We first describe the spectral identification and the derivation of the brightness of the emission features. Figure 2 presents the average brightness of the 23 calibrated disc and limb spectra in the wavelength range 90-120 nm, obtained as the UVIS FUV and EUV slits intersected the illuminated disc. The most intense spectral feature common to the EUV and FUV channels is the 115.2 nm emission which is a blend of the CO B-X Hopfield-Birge (0-0) band and OI emissions. Because of the rapid loss of sensitivity of the FUV channel near its short wavelength limit due to the sharp decrease of the MgF2 transmission curve, the FUV channel is difficult to calibrate near 115 nm. Hence, we chose to keep the 115.2 nm emission from the EUV channel and have merged the EUV and FUV spectra at 115.3 nm, where the red wing of this peak is near its minimum value. Features belonging to OI, OII, HI, NI, CI and CO are identified based on the wavelength list for atomic transitions by Ralchenko et al. (2008) and guided by the HUT Venus spectrum and the high-resolution (0.02 nm) spectrum of Mars obtained with the Far Ultraviolet Spectroscopic Explorer (FUSE) satellite in the 90.5-118.7 nm spectral range (Krasnopolsky and Feldman, 2002). The FUSE FUV spectrum of Mars, degraded to the spectral resolution of the UVIS EUV channel, is also shown in Figure 2 for comparison. We take advantage of the unambiguous identification of the Mars dayglow features by Krasnopolsky and Feldman which was made possible by the high spectral resolution and signal to noise ratio of the FUSE spectrum. A comparison of the two spectra indicates that most features are common to the two planetary EUV airglows, although the relative brightness of the emissions may be somewhat different. A noticeable difference is the absence of the argon lines at 104.8 and 106.7 nm in the Venus spectrum. Figure 3 shows the UVIS Venus spectrum between 80 and 130 nm, together with the spectral identifications. The intensities of several UVIS emissions measured across the disc, excluding the last few records collected near the sunlit limb, have been averaged to determine the average disc emission rates and are listed in **Table 2**. They range from 261 R for the OII 83.4 nm emission down to a few Rayleighs for the weaker emissions. The one-sigma standard deviation levels are also listed and correspond to the statistical photon noise of the accumulated spectrum only. The emissions from 112.2 to 130 nm discussed in this paper are affected by the very intense Ly-α wings. We therefore chose to report the intensity of these emissions above the instrumentally produced Lyman-α line wing, thus excluding the underlying instrumentally produced signal due to the Lyman-α wing and the contribution of blended weak emissions. In order to keep homogeneous values along this study, this method has been extended to all the features discussed in the paper. The intensity we provide should therefore be considered as lower limit values.

The OII ($2p^4\ ^4P$ - $2p^3\ ^4S$) triplet at 83.4 nm clearly stands as the brightest feature in the EUV spectra below 110 nm. This feature has been is observed in the spectrum of the terrestrial dayglow (~600 R) where it is predominantly excited by photoionization of ground-state $O(^3P)$ atomic oxygen requiring an energy of 14.9 eV. Most of the photons are emitted in the lower thermosphere and upward traveling photons suffer multiple scattering when they cross the ionospheric F-region. On Venus, this emission is also optically thick and multiple scattering occurs above ~200 km, where O^+ becomes the dominant ion in the daytime ionosphere. The disc average intensity is 261 R for the high solar activity conditions of the Cassini flyby. It was 91 R in the HUT spectrum near solar minimum when the $F_{10.7}$ cm index was 82. The Venera 11 measurements (Bertaux et al., 1981) gave a maximum disc value of 156 R for a moderate $F_{10.7}$ index of 138, with 20% variations observed across the disc. The variation of this emission across the disc and its comparison with model calculations will be discussed in further details in section 5.

A weak feature appears to be present at slightly above the noise level near 91 nm. A possibility is the NI 2p3 ^{4}S-2p2(^{3}P)5s ^{4}P multiplet at 91 nm which is observed in the terrestrial dayglow spectrum with an intensity of about 90 R and possibly also observed in the high-resolution FUSE spectrum of Mars. A second feature, the 2s^2 2p2 ^{3}P-2s2p3 ^{3}P° sextuplet, is possibly present at 91.6 nm . No ArII emission at 91.9 nm is measured above the noise level. Assuming that the average intensity of 30 R/nm in the 91-93 nm range is background noise, the upper limit intensity of the 91.9 nm ArII line is ~11 R. Its absence is consistent with the Venus HUT spectrum where this emission was weaker than the sensitivity threshold of 4 R. The weak emission at 97.3 nm is probably a blend of the Ly-γ line at 97.25 nm and the 2s^{2}2p^4 3P- 2s^{2}2p^3(4S°) 4d^{3}D° OI triplet at 97.17, 97.32 and 97.39 nm. The weak feature at 98.0 nm is coincident with the wavelength of the N_2 Caroll-Yoshino (CY) (0-1) band which is also observed in the Earth's (Bishop et al., 2007) and Mars (Krasnopolsky and Feldman, 2002) dayglow spectrum. The observed disc brightness in this UVIS spectrum is about 4 R.

The OI (2p4 ^{3}P - 3s' ^{3}D°) sextuplet at 98.9 nm is another prominent emission of the EUV spectrum, consisting of a triplet, a doublet and a singlet. It is also a bright feature of the Earth's dayglow where its production is dominated by photoelectron impact, in the absence of any strong solar emission at this wavelength, according to Meier (1991). The optically thick OI 2p^4 ^{3}P - 3d ^{3}D° intercombination sextuplet at 102.7 nm is blended at the UVIS spectral resolution with the Ly-β transition at 102.57 nm, which is coincidentally resonant with the three transitions of the multiplet originating from the J = 2 level of the ground state feeding photons into the total multiplet. According to Meier et al. (1987), in the terrestrial dayglow, some 85% of the OI emission is expected to be in the OI singlet transition at 102.816 nm. In the FUSE Mars spectrum, the OI 102.7 nm intensity was estimated assuming that the three components of the multiplet are distributed according their statistical weight. In this case, the OI multiplet accounts for 57% of the blended feature.

The feature near 104.nm is identified as the OI $2s^22p^4\ ^3P$ - $2s^22p^3(^4S^\circ)4s\ ^3S^\circ$ multiplet transition leading to the $O(^3P)$ ground state. This triplet is present and spectrally resolved in the FUSE Mars spectrum. Krasnopolsky and Feldman (2002) indicate that, as for the 97.2 nm triplet, the relative emergent intensity of the three components is very different from the statistical weight ratio, implying the presence of strong multiple scattering. This is confirmed by the absence of a pronounced limb brightening in the UVIS spatial scan at this wavelength. The ArI emissions at 104.8 and 106.7 nm, which are among the strongest EUV features in the FUSE Mars spectrum, are not distinguished from the noise level, setting up an upper limit of ~11 R.

The emissions at 107.5 and 106.8 nm are identified as the (0-0) E-X and C-X Hopfield-Birge bands of carbon monoxide respectively, also present in the FUSE Mars spectrum. The C-X band is possibly partly contaminated by the NII ^3P-$^3D^\circ$ sextuplet at 108.4-108.6 nm. The B-X, C-X and E-X transitions between singlet states are similar to the Fourth Positive bands connecting the CO ground state to the A $^1\Sigma$, B $^1\Sigma$ and C $^1\Sigma$ state. The C-X (0-0) band is optically thick and subject to intense self-absorption (Feldman et al., 2000). Both the C-X and the B-X emissions will be compared with model predictions in section 5.5.

The weak emission observed near 109.7 nm is present in individual spectra. We identify it as the triplet belonging to the NI $2s^22p^3\ ^2D^\circ$ - $2s^22p^2(^3P)4d\ ^2F$ transition. This feature was not present at any measurable level in the HUT Mars spectrum but it was observed in the terrestrial airglow by Gentieu et al. (1981) with a brightness of ~250 R. The emission near 111.4 nm was not identified in the HUT Venus airglow spectrum but we attribute it to the set of CI lines also observed at this wavelength in the FUSE Mars spectrum. Its average disc brightness is 14 R above the noise level and the intensity at the limb reaches ~40 R. The NI $2s^22p^3\ ^4S^\circ$ - $2s^22p^4\ ^4P$ triplet at 113.4 nm and the other features up to 130 nm are superimposed on the signal caused by Ly-α scattered light. The NI 113.4 nm triplet was observed on Mars by FUSE with a total disc brightness of ~3 R, of 35 ± 11 R by HUT on Venus and 585±45 R by HUT in the terrestrial atmosphere where it is predominantly excited by electron impact on N atoms (Bishop and Feldman, 2003). In the UVIS spectrum, this feature has a disc brightness of ~27 R.

The B-X Hopfield-Birge (0-0) band at 115.1 nm was first observed in the Venus HUT spectrum together with the (0-1) band at 112.4 nm. According to Krasnopolsky and Feldman (2002), the B state is mostly populated by electron impact excitation on CO molecules. Unlike the C state, fluorescence appears to contribute only weakly to the excitation of the CO B state. Both B-X and C-X bands are also present in the EUV spectra of several comets (Feldman, 1985). The OI $2p^4\ ^1D$ – $3s'\ ^1D^\circ$ line at 115.22 nm is blended with the strong B-X CO (0-0) band at the UVIS resolution. It was resolved from the B-X (0-0) bands in the FUSE Mars spectrum where the OI disc brightness is 11.1 R, compared to 16.6 R for the B-X (0-0) band. If the same intensity ratio is adopted for Venus, the B-X (0-0) band is estimated at 126 R and the OI ^1D-$^1D^\circ$ line at 85 R. Since the intensity of the B-X (0-1) band at 112.4 nm is only a few percent of the (0-0) band, its estimated brightness is less than 5 R. In the UVIS spectrum no emission feature is clearly discernable against the background signal at the position of the 112.4 nm band. We note that the C-X/B-X intensity ratio is more than twice as high in the UVIS spectrum than in the HUT spectrum.

The emission near 115.8 nm probably results from an accumulation of lines belonging to different CI and CII transitions. It was observed in the FUSE spectrum of Mars (Krasnopolsky and Feldman, 2002) and comets (Feldman, 2005). Most of the brightness in the Mars spectrum was ascribed to the carbon multiplet near 115.7 nm. Its average Venus disc brightness is on the order of 13 R. Two weak emissions are observed near 118.9 and 119.2 nm. The feature at 119.2 nm was also observed in the HUT spectrum of Venus, but was not identified. We speculate that this is the NI $2s^22p^3\ ^2P°$- $2s^22p^2(^3P)5d\ ^2P$ multiplet at 119.1 nm observed in the EUV spectrum of the Earth's dayglow by Gentieu et al. (1979).

The NI ^4S-^4P resonance triplet at 120.0 nm is clearly observed above the Ly-α stray light contribution. The intensity amounts to value of ~93 R. HUT measurements of the terrestrial dayglow give an intensity of 2090±80 R, with a production rate dominated by photodissociative excitation of N_2, followed by electron impact on N atoms and N_2 molecules. Excitation processes and the effect of multiple scattering will be discussed in section 5. The feature at 124.3 nm corresponds to the NI $2s^2\ 2p^3\ ^2D°$ - $2s^22p^2(^1D)$ 3s ^2D transition. It is present in terrestrial FUV dayglow with a nadir brightness of 155 R (Bishop and Feldman, 2003), where it is excited by photodissociative excitation and electron impact dissociative excitation of N_2. The CI sextuplets observed at 126.1 ($2s^22p^2\ ^3P$ - $2s^22p(^2P°)3d\ ^3P°$ transition) and 127.7 nm ($2s^22p^2\ ^3P$ - $2s^22p(^2P°)$ 3d $^3D°$ transition) are also observed in the Venus HUT spectrum.

At longer wavelengths, most features are blended with the optically thick CO($A^1\Pi \rightarrow X\ ^1\Sigma$) Fourth Positive (4P) bands, as discussed by Hubert et al. (2010). This is the case for the CI multiplets at 156.1 and 165.7 nm and the OI triplet at 135.6 nm. Analysis of these carbon emissions requires the development of a model of the carbon density in the Venus thermosphere and is left for a later study.

4. Comparison with HUT observations and spatial scans

Table 2 compares the UVIS average disc intensity of a series of emissions with the measurements by *Feldman at al.* (2000). They listed the average brightness of 13 emissions identified within their spectral range of 82-184 nm obtained with HUT from the Space Shuttle Astro 2 mission on 13 March 1995. The HUT Venus observations were made when the planet was at a western elongation of 40° and a phase of 60°. The UVIS observations were collected at a phase angle close to 99°. The HUT spectrum integrated the full Venus disc, but only the sunlit fraction, contributed to the dayglow emissions. As was shown in Figure 1, UVIS observed only a narrow strip of the planet extending from the dusk terminator to the vicinity of the subsolar limb. The solar activity was low for HUT, with an estimated F10.7 index of 82, and very high during the UVIS flyby (F10.7 = 214). It must also be noted that the observing geometries of HUT and UVIS were different, as the UVIS line of sight remained strongly inclined with respect to the zenith direction during the whole flyby. At a tangent altitude of 140 km altitude, the emission angle from UVIS line is always larger than ~45°. Nevertheless, both sets of brightnesses are in good agreement, with UVIS intensities generally higher than the HUT values, as expected from the higher solar activity level during the UVIS flyby. Table 2 indicates that the intensity ratios in the two sets of observations vary from 1.2 to 2.9 and tend to decrease from the EUV to the FUV, as a consequence of the growing role played by short EUV and X-ray solar emission in the excitation of higher lying levels (shorter wavelengths), combined with the increasing modulation of solar line intensities by the solar cycle at shorter wavelengths. An exception is the CO B-X (0-0) band which is blended with the OI multiplet at 115.2 nm, for which the precise spectral range covered by the molecular band is difficult to estimate.

We now examine the intensity distribution of a few EUV emissions measured along the slit scan of the Venus disc during the Cassini flyby. Figure 4 shows the observed intensities as a function of the solar zenith angle for the following emissions: OII 83.4 nm, OI 98.9 nm, Ly-ß + OI 102.5 nm, CO C-X (0-0) band + NII 108.8 nm, CO B-X + OI 115.2 nm and NI 120.0 nm. Table 3 lists the solar zenith and the emission angle corresponding to each record. The level of limb brightening is most pronounced for the OI 83.4 nm emission. By contrast, the OI multiplet at 98.9 nm and the CO C-X emissions only show a moderate increase as the UVIS slit crosses the planetary limb. The level of limb brightening is indicative of the amount of multiple scattering encountered by the photons on their way to escape the atmosphere.

5. Modelling the dayglow emissions

5.1 The model

The numerical model described by *Shematovich et al.* (2007 has been used to calculate the photoelectron production and energy degradation in the Venus atmosphere. Results from this model were favorably compared with ultraviolet spectra of Venus obtained with the PV-OUVS instrument (*Gérard et al.*, 2007) and of Mars collected with the SPICAV spectrograph (*Shematovich et al.*, 2007; *Hubert et al.*, 2010). Energetic electrons are produced by photoionization of the major atmospheric constituents by EUV and X-ray solar radiation. These photoelectrons are transported in the thermosphere where they lose their kinetic energy in elastic, inelastic and ionization collisions with the ambient atmospheric gas. The Direct Simulation Monte Carlo (DSMC) method is used to solve atmospheric kinetic systems in the stochastic approximation. The lower boundary is set at an altitude 100 km and the upper boundary is fixed at 250 km. This region is divided into 49 vertical cells. The excitation rates of the various upper states by electron impact are then directly calculated using the calculated energy distribution function, the target density distribution and the relevant excitation cross sections. If they significantly contribute, the contribution of the photo-excitation processes are then added as sources of excited atoms. The solar UV flux, corrected for the Sun-Venus distance, is obtained from the SOLAR2000 (version 2.27) empirical model (*Tobiska*, 2004) for the date of the Cassini swingby. The angle between Venus, the Sun and the Earth is used to account for the difference in the face of the Sun seen by Earth and Venus. The number densities of CO_2, CO, O, N_2 and N are provided by the VTS3 empirical model (*Hedin et al.*, 1983). Many of the emissions identified in the UVIS spectra are optically thick. The effect of multiple scattering on the 83.4 nm, 98.9 nm and 120.0 nm optically thick emissions is calculated using the resonance line radiative transfer code described by *Gladstone* (1985). The process of frequency redistribution allows photons to escape an optically thick atmosphere by scattering in frequency from the core of the line into the optically thin line wings. In this study we use angle-averaged partial frequency redistribution. The role of spherical geometry becomes important for viewing and solar zenith angles larger than ~70°. It is accounted for in the radiative transfer code to calculate the photon slant optical paths. The solar flux is obtained from the model of Woods and Rottman (2002) that sets up a proxy relating the solar UV flux and the F10.7 index. We note that the model provides the calculated integrated intensity along the line of sight. However, at the limb the observed signal is averaged over the size of the projected UVIS slit. This effect in not accounted for in the comparisons presented here, so that the amount of limb brightening is overestimated in the model.

In this study, we only model the brightness distribution across the disc for those emissions which are bright enough to yield a reliable signal to be compared with the model output. We also do not attempt to model the 102.7 nm multiplet, which is a blend of HI Ly-ß and OI emissions where the components of the OI multiplet are mixed and whose understanding in the terrestrial dayglow is not currently satisfactory. Under these circumstances, it appears that the determination of any result about the Venus atmospheric composition or structure based on this emission would be very illusive. For these reasons, we concentrate on the emissions of O^+ emission at 83.4 nm, the OI multiplet at 98.9 nm, the NI multiplets at 113.4, 120, and 124.3 nm and the Hopfield-Birge B-X (0-0) and C-X (0-0) bands. The calculated disc-averaged intensities of several features are listed in Table 2 and will be discussed in the next sections.

5.2 O^+ emission at 83.4 nm

In the Earth's atmosphere, the $O^+(^4P)$ atoms are mostly excited by shell ionization of ground state $O(^3P)$ atoms, with additional contributions from photoelectron impact on O atoms and resonance scattering of solar EUV radiation (Meier, 1991; Link et al., 1994):

$$\begin{aligned} &O + h\nu \rightarrow O^+(^4P) \\ &O + e \rightarrow O^+(^4P) + 2e \qquad (1) \\ &O^+ + h\nu \rightarrow O^+(^4P) \end{aligned}$$

It is estimated that about 95% of the excitations into the ^4P level are caused by electron impact ionization in the terrestrial dayglow. Radiative transfer through the F region plays an important role when the 83.4 nm photons cross the upper ionosphere and are resonantly scattered by the thermal population of O^+ ions. It is expected that a similar situation occurs in the Venus thermosphere where the bulk of the $O^+(^4P)$ atoms are produced by excitative photoionization near 140 km and upward going 83.4 nm photons cross an optically thick layer of O^+ ions in the upper thermosphere. Downward emitted photons are lost by absorption in CO_2. The contribution from solar resonance scattering to the intensity calculated for the UVIS observing conditions is only on the order of 0.3 % only and can thus be neglected. Figure 5 shows the contributions to the volume excitation rate of $O^+(^4P)$ ions modeled for a solar zenith angle of 64°, corresponding to UVIS record #25 with the smallest emission angle of the UVIS equal to 47° (see Table 3). We show the primary excitation rate (thin lines) and the radiative transfer source functions accounting for multiple scattering (thick lines). The O^+ density profile is obtained by interpolating the calculations of Fox and Sung (2001) versus the $F_{10.7}$ index. The dependence versus the solar zenith angle is estimated based on the ion density measurement from Pioneer Venus presented in Figure 13b of Brace and Kliore (1991), which is used to scale the density profile interpolated from Fox and Sung for a 0° solar zenith angle, taking z = 270 km as a reference for the whole density profile, and assuming that O^+ ions dominate by far the density of other ions. Radiative transfer is calculated using the cross sections and oscillator strength values for the multiplet given by Link et al. (1994). To compare the observed intensity variation across the Venus disc measured by UVIS with our model calculations, Figure 6a shows the comparison between the observed and the calculated intensity along the UVIS slit track. The calculated intensity exceeds the observation by roughly a factor of 2, an acceptable result considering the sources of uncertainties, and especially the poor knowledge of the O^+ density profile for the conditions of the Cassini flyby and the high variability of the Venus topside ionosphere. We thus also carried out a sensitivity study versus the O^+ density profile which was scaled by factors 2, 5 and 10. Figure 6a also shows the results obtained for these modified O^+ profiles. A better agreement is obtained when the O^+ density is multiplied by a between 5 and 10. This dependence against the O^+ density stems from the more efficient entrapment of the 83.4 nm radiation by an optically thicker O^+ ion layer in a region of the Venus atmosphere where it can be absorbed by CO_2. This results in the removal of photons absorbed by the CO_2 molecules, and thus in a lower model intensity. The larger optical thickness also reduces the limb brightening, in better agreement with the observations, although the observed limb brightening cannot directly be compared with the model, as mentioned before. In an optically thin layer, limb brightening is produced when the line of sight has a tangent point within the emitting layer, resulting in more photons contributing to the slant intensity. When the atmosphere is optically thick, one can consider, as a first approximation, that the line of sight is screened at a $\tau = 1$ distance, the optical thickness τ being computed along the line of sight from the observer location. If $\tau = 1$ is reached between the tangent point and the observer, this strongly reduces the limb brightening effect by limiting the length of the line of sight. The smaller amount of limb brightening in the UVIS observations suggests that a large column density of O^+ ions was present along the line of sight of the instrument. Nevertheless, an increase by an order of magnitude is a large factor, and we suspect that other unidentified factors may also possibly contribute to limiting the limb brightening and lowering of the intensity along the track on the planet. Admitting the possibility that the absolute calibration may be uncertain at this wavelength, a combination of 2 times the modeled O^+ density (i.e. the dashed curve in Figure 6a) and a UVIS effective area of 65-70% of the adopted value provides an even better fit to the observed spatial scan.

5.3 OI emission at 98.9 nm

The OI emission at 98.9 nm is a sextuplet composed of a singlet, a doublet and a triplet without mixing between the components (Meier, 1991). Atomic constants to calculate the effect of multiple scattering are taken from Bishop and Feldman (2003). The upper state also feeds the 799.0 nm emission but the branching ratio is small and, therefore, forbidden transitions such as the (3s' $^3D°$ - $2p^4$ ^1D) transition at 117. 2 nm must also be taken into account. Fitting of the nadir HUT terrestrial spectrum has led to the adoption of 3.8×10^{-4} and 1.1×10^{-4} for the values of the total branching ratio to other than the ground state and for the 117.2 nm fluorescence, respectively. In the Earth's thermosphere, the dominant excitation process is photoelectron impact on O atoms since the solar flux is small at this wavelength. A major difference appears to exist between the direct excitation and the emission cross sections. The source of this discrepancy has not been definitely identified (Gladstone et al. 1987) and the discussions about possible explanations will not be repeated here. We adopt the conclusion by Bishop and Feldman (2003) who scaled the cross section of Zipf and Erdman (1985) by a factor of 0.4, bringing it in close agreement with Vaughan and Doering's (1987) measurement, to match the observed Earth's 98.9 nm dayglow intensity. The other two processes contributing to the excitation of the ^3D state are dissociative excitation of CO_2 and CO by photoelectrons. The corresponding electron impact cross section are adopted from Kanik et al. (1993) and James et al. (1992). Figure 7 shows the contribution of the different photoelectron excitation sources and indicates that photoelectron impact on O atoms and CO molecules dominates over the CO_2 source.

Calculations for the UVIS flyby conditions lead to a total estimated vertical emission rate of ~12.6 R, 5.3 R of which being absorbed by CO_2 in calculations ignoring multiple scattering, a value much less then the observed disc averaged intensity of 110 R. We have therefore examined the possibility that resonance scattering of the solar EUV radiation significantly contributes to the excitation of the 98.9 nm multiplet. We use the solar flux proxy from Rotman and Moos (1973) to estimate the solar flux consistent with the F10.7 activity index corresponding to the UVIS observations. This proxy has a spectral resolution of 0.5 nm, too poor to discriminate the individual contribution of the 98.9 nm multiplet. From the high spectral resolution model of Tobiska (2004), we estimate that the 98.9 nm emission contributes ~27% to the solar intensity between 98.5 and 100.5 nm for high solar activity conditions. For comparison, the 98.9 nm contribution to the quiet sun high resolution solar spectrum by Curdt et al. (2001) in the same wavelength interval amounts to 19%, i.e. a comparable fraction. The detailed line shape of the solar 98.9 nm is not well known. We thus represent it assuming it has the shape of two offset Gaussians, and that the offset and FWHM of these Gaussians can be taken as the average parameters determined by Gladstone (1992) for the components of the OI 130.4 nm multiplet. Figure 8 shows the contributions to the volume excitation rate of excited O(^{3}D) atoms modeled for a solar zenith angle of 64°, corresponding to UVIS record #25 with the smallest emission angle of the UVIS equal to 47°. We show the primary excitation rate (thin lines) and the radiative transfer source functions accounting for multiple scattering (thick lines). We note that the resonance scattering contribution is larger than the photochemical sources.

The calculated intensity is 91 R for the solar activity conditions prevailing at the time of the UVIS observations (record 25). Figure 6b compares the observed 98.9nm intensity variation measured by UVIS with our model calculations. We estimate that the uncertainty on the measured 98.9 nm amounts to ~15-20 R, considering the random variations of the observed intensity along the track. The main source of OI 98.9 nm photons in the Venus thermosphere is found to be resonance scattering of solar photons, which has an uncertainty on the order of 20%. In our calculations, the photochemical sources of 98.9 photons are quite marginal, contributing ~5% of the total.

5.4 NI emissions at 113.4, 120.0 and 124.3 nm

The following processes may lead to the production of excited nitrogen atoms N*:

$$\begin{aligned}
&N_2 + h\nu \rightarrow N^* + N^{(+)} \quad (+\,e)\\
&N_2 + e \rightarrow N^* + N^{(+)} + e \quad (+\,e)\\
&N(^4S) + e \rightarrow N^* + e\\
&N(^4S) + h\nu \rightarrow N^* \quad (\textit{for resonance lines})
\end{aligned} \qquad (2)$$

We first consider the NI emission at 124.3 nm that is excited by N_2 photodissociation and photoelectron impact on N_2. The lower electronic state of the quadruplet is excited, so that multiple scattering does not play any role. We adopt the cross section for electron impact dissociative excitation by Tabata et al. (2006) and the photodissociative excitation cross sections by Wu (1994) scaled with the branching ratio for excitation of the $N(^2D)$ state by Samson et al. (1991). We find that the photodissociation source is dominant at altitudes above ~130 km. We calculate an intensity rate of 10 R for the geometry of UVIS record 25 (emission angle = 47°), a value 50% smaller than the observed values of 20 R for the 124.3 nm multiplet. Comparing the full disc value, the UVIS observation gives 23 ± 1 R, while our computation gives ~16 R.

The sextuplet at 113.4 nm is a resonant transition, but the optical depth is less than for the 120.0 nm multiplet. The major sources are photoelectron impact on N_2 and N and electron impact on ground state N atoms (reactions 2), with a possible contribution of resonance scattering of solar radiation. We use the cross sections by Doering and Goembel (1992) and by Tabata et al. (2006) for N and N_2 respectively, and the photodissociative excitation cross sections by Wu (1994) scaled with the branching ratio for excitation of the $N(^4P)$ state by Samson et al. (1991). The main peak is produced by N_2 photodissociation, followed by electron impact on N atoms. Photoelectron impact on N_2 only becomes important below 130 km, a region where photons are readily absorbed by CO_2. The emergent intensity calculated for UVIS record 25 is ~17 R. For the disc, we compute a brightness of 18.1 R to be compared with an observed value of 35 R.

The 120 nm multiplet is composed of three lines spaced by 0.067 and 0.049 nm. The excitation processes are the same as for the 113.4 nm multiplet. The solar spectrum is weak at 120.0 nm, so that resonance scattering of solar radiation is generally neglected as a source of primary production of N(^{4}P) atoms. In the terrestrial airglow, Bishop and Feldman (2003) found that photodissociative excitation of N_2 is the major source of N(^{4}P) excited atoms. However, to reach agreement with the HUT observations, they had to decrease the model N(^{4}S) density and scale the (renormalized) Stone and Zipf (1973) cross sections by a factor of 0.6. In this model calculation, we adopt the excitation cross section for N_2 photodissociation by Wu (1994), the electron impact cross section on N_2 by Tabata et al. (2006) and the electron impact cross section on N atoms by Doering and Goembel (1991). The contribution of solar resonance scattering is calculated using the set of atomic parameters by Bishop and Feldman (2003) and the N(^{4}S) number density distribution by Hedin et al. (1983). The photochemical contributions to the N(^{4}P) excitation rate are shown in Figure 9. Photodissociative excitation of N_2 is clearly the dominant source of N(^{4}P) atoms. A second peak is predicted at lower altitude for electron impact on N_2 and N as a result of ionization by X-rays. The calculated column photochemical production rate of N(^{4}P) atoms through this process is ~7.8 x 10^7 cm^{-2} s^{-1}, which would correspond to a vertical intensity of 78 R if the atmosphere was optically thin.

Multiple scattering is calculated using the N(^{4}S) density vertical distribution given by the VTS3 empirical model. Using this distribution and the scattering cross section at the core of the brightest multiplet component, the optical depth at the emission peak is estimated on the order of 50. However, the N(^{4}S) fragments are hot atoms which emit the 120.0 nm radiation with a line width much higher than the width of the absorption by ambient N(^{4}S) atoms. Consequently, little multiple scattering is expected to occur from this source and the contribution of photons produced by N_2 dissociation should be optically thin (Meier, 1991). In our calculations, we assume that only 120-nm photons produced by photoelectron impact on N and by resonance scattering are scattered by N(^{4}S) atoms. Figure 10 shows the NI 120.0 nm primary source function for these two processes (thin lines) and the corresponding radiative transfer source function following multiple scattering (thick lines). We note the amplification by about two orders of magnitude caused by the optical thickness of the transition. Figure 6c compares our modeled NI 120 nm intensity with the UVIS observation. It must be stressed that the observed NI 120 nm brightness is strongly contaminated by the nearby very bright Lyman-α emission. This implies that the NI 120 nm brightness may be affected by a large uncertainty due to the difficult removal of the Lyman-α contaminant signal. Resonance scattering of sunlight contributes ~25% of the total computed brightness. The calculated total brightness exceeds the observations by about 80%, reduced to 30% if resonance scattering is neglected. If all sources were considered as optically thick, the calculated limb scan would significantly overestimate the 120.0-nm intensity and the shape of the distribution across the planetary disc would be in disagreement with the observations. We note that the emerging intensity of the 120.0 nm is largely insensitive to the $N(^4S)$ density profile used in the calculation. For example, in a simulation where the N density profile is reduced by a factor of 2, the calculated intensity decreases by only 10%. This small sensitivity to the abundance of N in the thermosphere stems from the relatively small contribution of the e + N and resonance scattering sources compared to the optically thin N_2 photodissociation sources. A better agreement with the UVIS observations would be reached with lower N_2 densities.

Comparing the intensity of the three atomic nitrogen emissions from Table 2, we find that the 120.0 nm/124.3 nm observed ratio is 4.0 and the 113.4 nm/124.3 nm ratio is 1.2. Our calculated ratios for the disc are 15.2 and 1.1 respectively. Interestingly we note that, in their Fig. 9, Bishop and Feldman give calculated intensity ratios of these emissions for photodissociative excitation of N_2 in the Earth's airglow equal to 4.0 and 1.3 respectively, in excellent agreement with our observed values. If the contribution from electron impact on N_2 is added, their calculated intensity ratios are 7.2 and 1.4.

5.5 The B-X and C-X (0-0) Hopfield-Birge bands

We assume that the B state is mostly excited by photoelectron impact on ground state CO. Although the CO C state may also be produced by dissociative excitation of CO_2, no measurement of this cross section appears to be available in the literature. Fluorescence is believed to weakly contribute to the excitation of the B-X emission, unlike the C-X transition (Feldman et al., 2000). Adopting the excitation cross section by Shirai et al. (2001), the calculated vertical column excitation rate for the B state is 1.15 $\times 10^8$ photons cm^{-2} s^{-1}. Laboratory measurements (Kanik et al., 1995) have shown that the branching ratio of the (0-0) bands of both B-X and C-X transitions is larger than 95%. We neglect self-absorption and adopt a unit branching ratio for the CO B-X (0-0) band. The calculated distribution of the excitation rates of the CO B and C states by electron impact on CO is displayed in Figure 11. The model predicts an emerging intensity of 163 R in the UVIS geometry for UVIS record 25. This value is in fair agreement with the observed intensity of 205 R. However, if the relative contribution of the OI multiplet at 115.21 nm is as large as to 60% as in the Mars FUSE spectrum, the model intensity for the B-X emission is ~93 R, in less satisfactory agreement than if all of the emission is ascribed to the Hopfield-Birge band.

The electron impact cross section for the C-X (0-0) band is significantly larger than for the B-X (0-0) band above 100 eV, but it is less at 20 eV (Kanik et al., 1995). The oscillator strength of the Hopfield-Birge C-X transition is about a factor of 18 larger than for B-X (Federman et al., 2001). Consequently, some lines in the (0-0) band are expected to be optically thick and self absorption may be important for this emission. Our model predicts a C-X emerging intensity of 37 R for the geometry of UVIS record 25. This value is twice less than the observed intensity of 70 R. Resonance fluorescence is a possible additional source of excitation of the C–X (0–0) band (Krasnoplolsky and Feldman, 2002).. As discussed before, some additional contribution from the OI 115.2 multiplet is expected at the UVIS spectral resolution.

Comparing the B-X and C-X emissions, the calculated column production rates for photoelectron impact on CO of the two band systems are nearly equal. However, the B-X band head has a unit optical depth for CO_2 absorption located at ~134 km, lower than the C-X band for which $\tau = 1$ is reached at ~148 km. This explains why the model predicts a B-X /C-X intensity ratio of 4.7, in reasonably good agreement with the observed ratio ranging between 4.8 and 3.4, depending whether a contribution of the OI multiplet is subtracted from measured intensity at 115.2 nm. We also note that the intensity of the E-X (0-0) band is about 4 R, that is 11 times as weak as the C-X emission. This ratio is in good agreement with the ratio of 12 of the peak cross section for 20-eV electron impact excitation of the E and C states (Kanik et al., 1995) .

The observed and modeled intensity distribution across the disc are shown in Figure 6d. The total measured intensity of the B-X (0-0) band across the disc is shown by the open circles. The values following subtraction of the estimated OI 115.2 nm emission contribution corresponds to the full circles. A better agreement with the observed disc brightness is obtained when the OI contribution is accounted for, with the exception of the limb intensity. The observed limb brightening is less than the model calculation in the absence of smoothing to account for the field of view. In addition, multiple scattering within the CO B-X (0,0) band is not accounted for in this comparison and the absorption cross section of CO_2 in the vicinity of these bands is large, rapidly varying and not experimentally determined at sufficient spectral resolution to make a detailed line-by-line calculation. Consequently, at this stage, further quantitative modeling of these emissions would be very uncertain.

6. Conclusions

We have analyzed the dayglow EUV observations collected with the UVIS instrument made during the flyby of Venus by Cassini at a 0.37 nm spectral resolution. Spatially resolved emissions belonging to OI, OII, NI, CI and CII have been identified, some of them for the first time in a Venus ultraviolet spectrum and their disc average intensity have been determined. They are generally somewhat brighter than those previously determined from the observations made with the HUT instrument. The difference is attributed to the higher solar activity prevailing during the Cassini flyby in comparison with those during the HUT observations.

The intensity distribution along the foot track of the UVIS slit of the OII 83.4 nm, OI 98.9 nm, Lyman-β + OI 115.2 nm and NI 120.0 nm multiplets and CO C-X and B-X Hopfield-Birge bands have been examined. They show different levels of limb brightening, depending on the optically thickness of the observed transition. A detailed comparison with the intensities along the slit track predicted by a detailed airglow model, including treatment of multiple scattering, has been made for the 83.4 nm, 98.9 nm, 120.0 nm multiplets and CO B-X (0,0) band. We find that the calculated intensity of the OII emission at 83.4 nm and the predicted amount of limb brightening are quite sensitive to the ionospheric content in O^+ ions. The observed brightness is weaker than predicted by the model if a standard distribution of O^+ ions is used in the radiative transfer calculation. An increase in the ion density by a factor of 5 to 10 brings the observations and the modeled values into agreement. The calculated intensity distribution of the OI 98.9 nm and CO B-X emission along the track of the UVIS slit is satisfactorily predicted by the model. A good agreement with the observed OI 98.9 nm emission is only obtained if resonance scattering of solar radiation by O atoms is included as a source. We note that this process dominates over the photochemical processes which are generally considered as the major contributions to the excitation of the O(^{3}D) state in the terrestrial dayglow. Finally, the intensity of the NI multiplet at 120.0 nm is somewhat overestimated by the model, but in better agreement with the observations if the hot N(^{4}S) atoms produced by N_2 dissociation do not contribute to the optical thickness of this transition. Simulations indicate that the intensity of the 120.0 nm emission only weakly depends on the thermospheric abundance of ground state N atoms. This emission, similarly to other EUV nitrogen lines, is mostly produced by dissociative excitation of N_2. It is therefore inadequate to probe the N dayside on the Venus dayside. Overall, we conclude that densities given by the VTS3 empirical model, coupled with the existing set of excitation cross sections, satisfactorily reproduce the ultraviolet dayglow observations performed with UVIS at low latitudes during a period of high solar activity. Further observations would be necessary to determine whether this conclusion also holds at low activity and higher latitudes.

Acknowledgements. This study is based on observations by the Cassini project. B. Hubert and J.-C. Gérard are supported by the Belgian National Fund for Scientific Research (FNRS) and V. Shematovich and D. Bisikalo by RFBR grant #08-02-00263. Funding for this research was managed by the PRODEX program of the European Space Agency in collaboration with the Belgian Science Policy Office and by FRFC grant #4.4508.06.

References

Ajello, J.M., et al., 2005. The Cassini Campaign observations of the Jupiter aurora by the Ultraviolet Imaging Spectrograph and the Space Telescope Imaging Spectrograph. Icarus. 178, 327-345, doi: 10.1016/j.icarus.2005.01.023.

Bertaux, J. L., Blamont, J. E., Lepine, V. M., Kurt, V.G., Romanova, N.N., Smirnov, A.S., 1981. Venera 11 and Venera 12 observations of E.U.V. emissions from the upper atmosphere of Venus. Planet. Space Sci. 29, 149-166.

Bishop, J., Feldman, P.D., 2003. Analysis of the Astro-1/Hopkins Ultraviolet Telescope EUV–FUV dayside nadir spectral radiance measurements. J. Geophys. Res. 108, 1243, doi:10.1029/2001JA000330.

Broadfoot, A.L., Kumar, S., Belton, M.J.S., McElroy, M.B., 1974. Ultraviolet Observations of Venus from Mariner 10: Preliminary Result. Science 183, 1315-1318.

Brace, L.H., Kliore, A.J., 1991. The structure of the Venus ionosphere. Space. Sci. Rev. 55, 81-163.

Curdt, W., Brekke, P., Feldman, U., Wilhelm, K. , Dwivedi, B. N., Schühle, U., Lemaire, P., 2001. The SUMER spectral atlas of solar-disk features. A&A, 375, 591–613, doi: 10.1051/0004-6361:20010364.

Doering, J.P., Goembel, L., 1991. Absolute differential and integral excitation cross sections for atomic nitrogen 1. The $^4S^0 \rightarrow 3s\ ^4P$ (1200 Å) transition from 30 to 100 eV. J. Geophys. Res. 96, 16021-16024.

Doering, J.P., Goembel, L., 1992. Absolute differential and integral electron excitation cross Sections for atomic Nitrogen, 2. The $^4S^0 \rightarrow 2p^4\ ^4P$ (Lambda 1134 Å) transition from 30 to 100 eV. J. Geophys. Res. 97, 4295-4298.

Esposito, L.W., Colwell, J.E., McClintock, W.E., 1998. Cassini UVIS observations of Saturn rings. Planet. Space. Sci. 46, 1221-1235, doi:10.1016/S0032-0633(98)00076-2.

Esposito, L.W. et al., 2004. The Cassini Ultraviolet Imaging Spectrograph investigation. Space Science Rev. 115, 299-361, doi: 10.1007/s11214-004-1455-8.

Federman, S. R., Fritts, M., Cheng, S., Menningen, K.M., Knauth, D.C., Fulk, K., 2001. Oscillator Strengths for B-X, C-X, and E-X Transitions in Carbon Monoxide, Ap. J. Supl. 134, 133-138.

Feldman, P.D, 2005. Spectroscopy of Comets with the Far Ultraviolet Spectroscopic Explorer satellite, Physica Scripta TI19, 7-12.

Feldman, P.D., Burgh E.B., Durrance S.T., Davidsen A.F., 2000. Far-ultraviolet spectroscopy of Venus and Mars at 4 Å resolution with the Hopkins Ultraviolet Telescope on ASTRO-2. Astrophys. J. 538, 395- 400, doi: 10.1086/309125.

Fox, J., Bougher, S.W., 1991. Structure, luminosity, and dynamics of the Venus thermosphere, Space Science Rev., 55, 357-489.

Fox, J., Sung. K., 2001. Solar activity variations of the Venus thermosphere/ionosphere. J. Geophys. Res. 106(A10), 21305-21335.

Gentieu, E. P., Feldman, P.D., Meier, R.R., 1979. Spectroscopy of the extreme ultraviolet dayglow at 6.5Å resolution: atomic and ionic emissions between 530 and 1240 Å. Geophys. Res. Lett. 6, 325-328

Gérard, J.-C., Hubert, B., Shematovich, V.I., Bisikalo, D.V., Gladstone, G.R., 2008. The Venus ultraviolet oxygen dayglow and aurora: Model comparison with observations. Planet. Space. Sci. 56, 542-552, doi:10.1016/j.pss.2007.11.008.

Gladstone, G.R., 1985. Radiative transfer of resonance lines with internal sources. J. Quant. Spectr. Radiat. Transfer 33, 453–458.

Gladstone, G.R., 1992. Solar OI 1304 Å triplet line profiles. J. Geophys. Res. 97, 19125–19519.

Gladstone, G.R., Link, R., Chakrabarti, S., McConnell, J.C., Modeling of the O I 989-Å to 1173-Å ratio in the terrestrial dayglow. J. Geophys. Res. 92, 12,445–12,450, doi:10.1029/JA092.

Hedin, A.E., Niemann, H.B., Kasprzak, W.T., Seiff, A., 1983. Global empirical model of the Venus thermosphere. J. Geophys. Res. 88, 73–83.

Hubert, B., Gérard, J.-C., Gustin, J., Shematovich, V.I., Bisikalo, D.V., Stewart, A.I., Gladstone, G.R., L. Esposito, 2010. Cassini-UVIS observations of the FUV OI and CO Venus dayglow. Icarus, doi:10.1016/j.icarus.2009.12.029, in press.

James, G. K., Ajello, J.M., Kanik, I., Franklin, B., Shemansky, D.E., 1992. The extreme ultraviolet emission spectrum of CO produced by electron impact at 20 and 200 eV. J. of Physics B 25, 1481-1496.

Kanik, I., Ajello, J.M., James, G.K., 1993. Extreme ultraviolet emission spectrum of CO_2 induced by electron impact at 200 eV. Chem. Phys. Lett. 211, 523-528.

Kanik, I., James, G.K., Ajello, J.M., 1995. Medium-resolution studies of extreme-ultraviolet emission from CO by electron impact. Phys. Rev A. 51, 2067-2074.

Krasnopolsky, V.A. Feldman, P.D., 2002. Far Ultraviolet spectrum of Mars. Icarus 160, 86-94, doi: 10.1006/icar.2002.6949.

Link, R., Evans, J., Gladstone G.,1994. The O^+ 834-Å dayglow: revised cross sections. J. Geophys. Res. 99, 2121-2130.

Meier, R.R., 1991. Ultraviolet spectroscopy and remote sensing of the upper atmosphere. Space Sci. Rev. 58, 1-185.

Meier, R.R., Anderson Jr., D.E., Paxton, L.J., McCoy, R.P., Chakrabarti, S., 1987. The OI 3d $^{3}D^{\circ}$ - 2p4 ^{3}P transition at 1026 Å in the day airglow. J. Geophys. Res. 92, 8767–8773, doi:10.1029/JA092iA08p08767.

Moos, H.W., Rottman, G.J., 1971. OI and HI emissions from the upper atmosphere of Venus. Astrophys. J. 169, L127.

Moos, H.W., Fastie W.G., Bottema, M., 1969. Rocket measurement of ultraviolet spectra of Venus and Jupiter between 1200-1800 Å. Astrophys. J. 155, 887-897.

Paxton, L.J. and Anderson, D.E., 1992. Far ultraviolet remote sensing of Venus and Mars, in Venus and Mars: Atmospheres, Ionospheres, and solar wind Interactions, AGU Geophysical Monograph 66, 113-189, American Geophysical Union, Washington D.C.

Ralchenko, Yu., Kramida, A.E., Reader, J., NIST ASD Team (2008). NIST Atomic Spectra Database (version 3.1.5), [Online]. Available: http://physics.nist.gov/asd3 [2010, February 19]. National Institute of Standards and Technology, Gaithersburg, MD

Rottman, G. J., Moos, H.W, 1973. The ultraviolet (1200-1900 angstrom) spectrum of Venus. J. Geophys. Res. 78, 8033.

Samson, J.A.R., Chung, Y., Lee E.-M., 1991. Excited ionic and neutral fragments produced by dissociation of the N_2^{+*} H band. J. Chem. Phys., 95, 717-719.

Shematovich, V.I., Bisikalo, D.V., Gérard, J.-C., Cox, C., Bougher, S.W., Leblanc, F., 2008. Monte Carlo model of the electron transport for the calculations of Mars dayglow emissions. J. Geophys. Res. 113, E02011, doi:10.1029/2007JE002938.

Shirai, T., Tabata, T., Tawara, H., 2001. Analytic cross sections for electron collisions with CO, CO_2, and H_2O relevant to edge plasma impurities. Atom. Data Nucl. Data Tables, 79, 143-184.

Steffl, A.J., Stewart A.I.F., Bagenal. F., 2004. Cassini UVIS observations of the Io plasma torus. I. Initial results. Icarus 172, 78.

Stewart, A.I., 1980. Design and operation of the Pioneer Venus orbiter ultraviolet spectrometer. IEEE Trans. Geosci. Remote Sensing GE18, 65–70.

Stewart, A.I., Barth, C.A., 1979. Ultraviolet night airglow of Venus. Science 205, 59-62.

Stone, E. J., Zipf, E.C., 1973. Excitation of atomic nitrogen by electron impact. J. Chem. Phys. 58, 4278, doi:10.1063/1.

Tabata T., Shirai T., Sataka M., Kubo H., 2006. Analytic cross sections for electron impact collisions with nitrogen molecules. Atom. Data Nucl. Data Tables 92, 375-406.

Tobiska, W.K., 2004. SOLAR2000 irradiances for climate change, aeronomy and space system engineering. Adv. Space. Res. 34. 1736–1746.

Vaughan, S., Doering, J. 1987. Absolute experimental differential and integral electron excitation cross sections for atomic oxygen, 3, The ($^3P \rightarrow {}^3D^\circ$) transition (989 Å) from 20 to 200 eV with improved values for the ($^3P \rightarrow {}^3S^\circ$) transition (1304 Å). J. Geophys. Res. 92, 7749-7752.

Woods, T., Rottman, G., 2002. Ultraviolet variability over time periods of aeronomic interest, atmospheres in the solar system: comparative aeronomy. In: Mendillo, M., Nagy, A., Waite, J.H. (Eds.), Geophysical Monograph 130. American Geophysical Union, Washington, DC, p. 221.

Wu, C.Y.R., 1994. Fluorescence excitation function of NI 1200-A and cross sections for fluorescence photon-photoion coincidence produced through photoexcitation of N_2. J. Geophys. Res., 99, 8971-8979.

Zipf, E.C., Erdman, P.W., 1985. Electron impact excitation of atomic oxygen: revised cross sections. J. Geophys. Res. 90, 11087-11110.

TABLE 1. UVIS spectrum of Venus

Date	24 June 1999
Total exposure time	13 min
Exposure time/record	32 s
Slit angular aperture	64 mrad
Spectral resolution	0.37 nm
Solar zenith angle	11° - >90°
Emission angle	47° - 83°
Phase angle	~99°
$F_{10.7\ cm}$ index (at Earth distance)	214

Table 2. Average brightness of selected spectral features of the Venus EUV and FUV: airglow disc intensities observed with UVIS (records 16 to 34), comparison with HUT observations and model calculations.

λ (nm)	Emissions	UVIS (R)	HUT (R)	UVIS/HUT ratio	Model (R)
83.4	OII	261±4	91±41	2.9	536
98.9	OI	110±2	45 ±33	2.4	94
102.5	OI + Ly-ß	180±3	115± 23	1.6	-
104.0	OI	25±1	25±1	1	-
108.8	CO C-X (0,0) + NII	44±6	63±2	1.4	37**
114.0	CI	14± 1	-	-	-
113.4	NI	27±1	35±11	0.8	18.1
115.2	CO B-X (0-0) + OI	211±6	128±10	1.6	177**
115.8	CI	13±3	-	-	-
120.0	NI	93±4	77±16	1.2	176
124.3	NI	23±1	-	-	15.9
126.1	CI	15±1	-	-	-
127.7	CI	175±3	-	-	-
135.6	OI	776*±7	605*±28	1.3	840

*Including blended CO Fourth Positive underlying bands.

**Calculated for photoelectron impact on CO.

Table 3. Geometry of UVIS observations of Venus

UVIS record	SZA (deg)	EMA (deg)
14	97.2	77.6
15	94.2	70.0
16	91.2	64.7
17	88.3	60.7
18	85.3	57.3
19	82.2	54.5
20	79.4	52.2
21	76.4	50.4
22	73.5	49.0
23	70.4	47.9
24	67.4	47.3
25	64.2	47.1
26	61.1	47.3
27	57.8	47.9
28	54.5	49.0
29	51.1	50.4
30	47.5	52.3
31	43.8	54.6
32	39.9	57.4
33	35.8	60.8
34	31.3	64.2
35	26.2	68.4
36	20.1	73.9
37	11.1	83.2

Figure captions

Figure 1. Sketch of the UVIS field-of-view across Venus during Cassini's swingby on June 24, 1999. The center of the disc is at 30° latitude, 0800 LT. The solid curves on the disc are the traces of the middle and the two ends of the UVIS FUV slit. The line-of-sight for the center of the slit is shown every 60 sec from closest approach - 600 sec to +60 sec, and also at the times of first and last contact with the disc. The lengths of the line-of-sight at first contact, closest approach, and last contact were 7700, 1200, and 3000 km.

Figure 2. Average EUV dayglow spectrum from 90 to 120 nm obtained by the UVIS spectrograph during the Cassini swingby of Venus (black line). It includes contributions from both the disc and the limb, from record 16 to record 38. For comparison, the Mars dayglow spectrum obtained with the Far Ultraviolet Explorer (FUSE) telescope is shown at the spectral resolution of the UVIS instrument (red curve).

Figure 3. Average EUV dayglow spectrum from 80 to 130 nm obtained by the UVIS spectrograph during the Cassini swingby of Venus. Various lines and molecular bands are identified and discussed in the text.

Figure 4. Variation of the emission rate (in R) observed with UVIS, following background subtraction of the brightest atomic and molecular EUV emissions as a function of the record number along the UVIS footprint. The disc-averaged intensities are listed in Table 2 and the geometric parameters for each record are listed in Table 3.

Figure 5. Model calculation of the primary volume production rate of the OII multiplet at 83.4 nm for the conditions of UVIS record 25 (thin lines). Photoelectron impact on O atoms is the dominant source of excited O^+ ions in the thermosphere. The contributions to the radiative transfer source functions following multiple scattering are show by the thick lines.

Figure 6. Comparison between intensities of four EUV emissions observed along the track of the UVIS slit and modeled values; (a) OII 83.4 nm, (b) OI 98.9 nm, (c) NI 120.0 nm, (d) CO B-X (0-0) band (see text).

Figure 7. Model calculation of the photochemical excitation rates of the $O(^3D)$ atoms giving rise to the 98.9 nm multiplet emission calculated for the conditions of UVIS record 25.

Figure 8 Model calculation of the primary volume production rate of the OI multiplet at 98.9 nm for the conditions of UVIS record 25 (thin lines). The contributions to the radiative transfer source functions following multiple scattering are show by the thick lines

Figure 9. Photochemical excitation rates of $N(^4P)$ atoms giving rise to the NI 120.0 nm multiplet emisssion calculated for the conditions of UVIS record 25.

Figure 10. Contributions of the optically thick sources to the source function of the NI 120.0 nm emission. The three thin lines correspond to the primary volume production rate. The contributions to the source functions following multiple scattering are show by the thick lines. The set of curves is calculated for the conditions of UVIS record 25.

Figure 11. Model calculation of the volume excitation rate of the CO Hopfield-Birge B-X (solid line) and C-X (dashed line) bands calculated for the conditions of UVIS record 25.

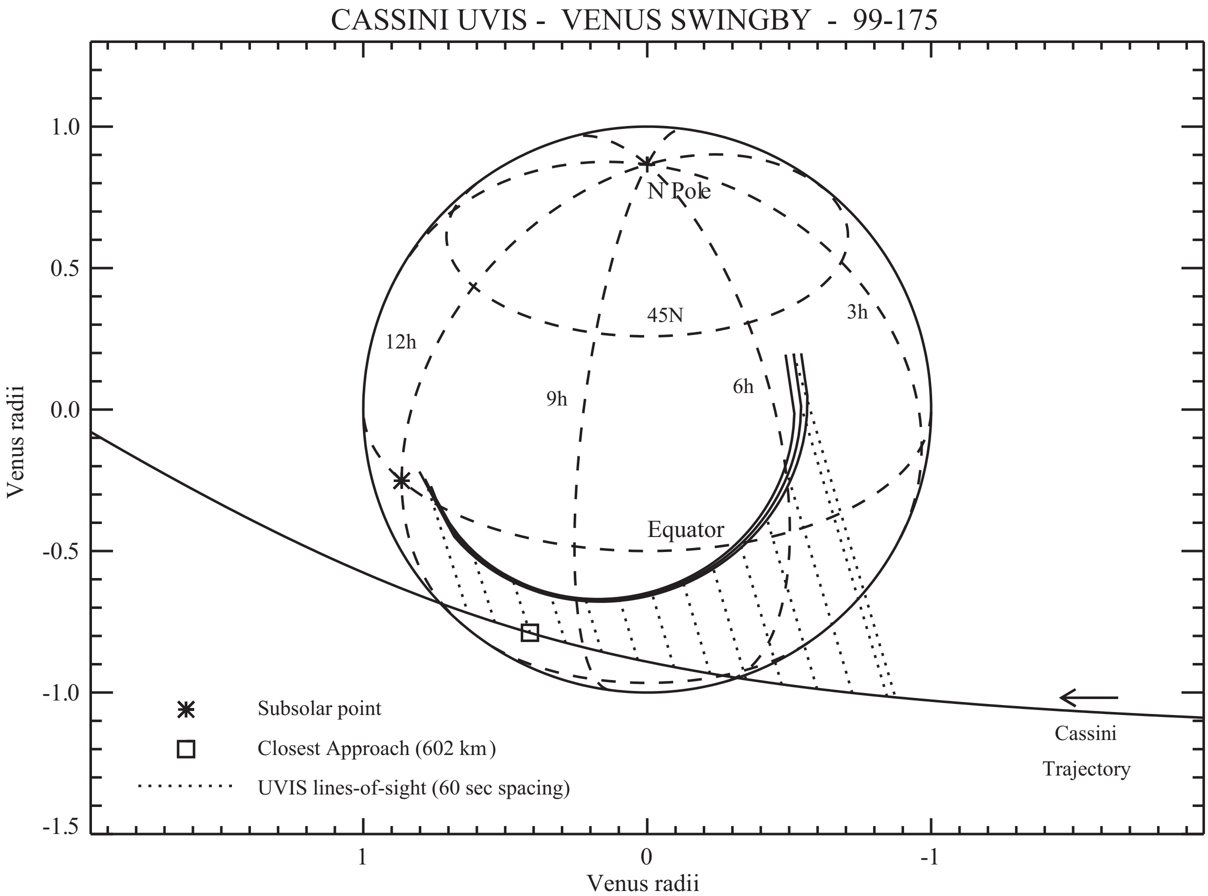
CASSINI UVIS - VENUS SWINGBY - 99-175
1.0
0.5
0.0
-0.5
-1.0
-1.5
Venus radii
1
0
-1
Venus radii
N Pole
45N
3h
12h
9h
6h
Equator
Subsolar point
Closest Approach (602 km)
UVIS lines-of-sight (60 sec spacing)
Cassini
Trajectory

Fig. 1

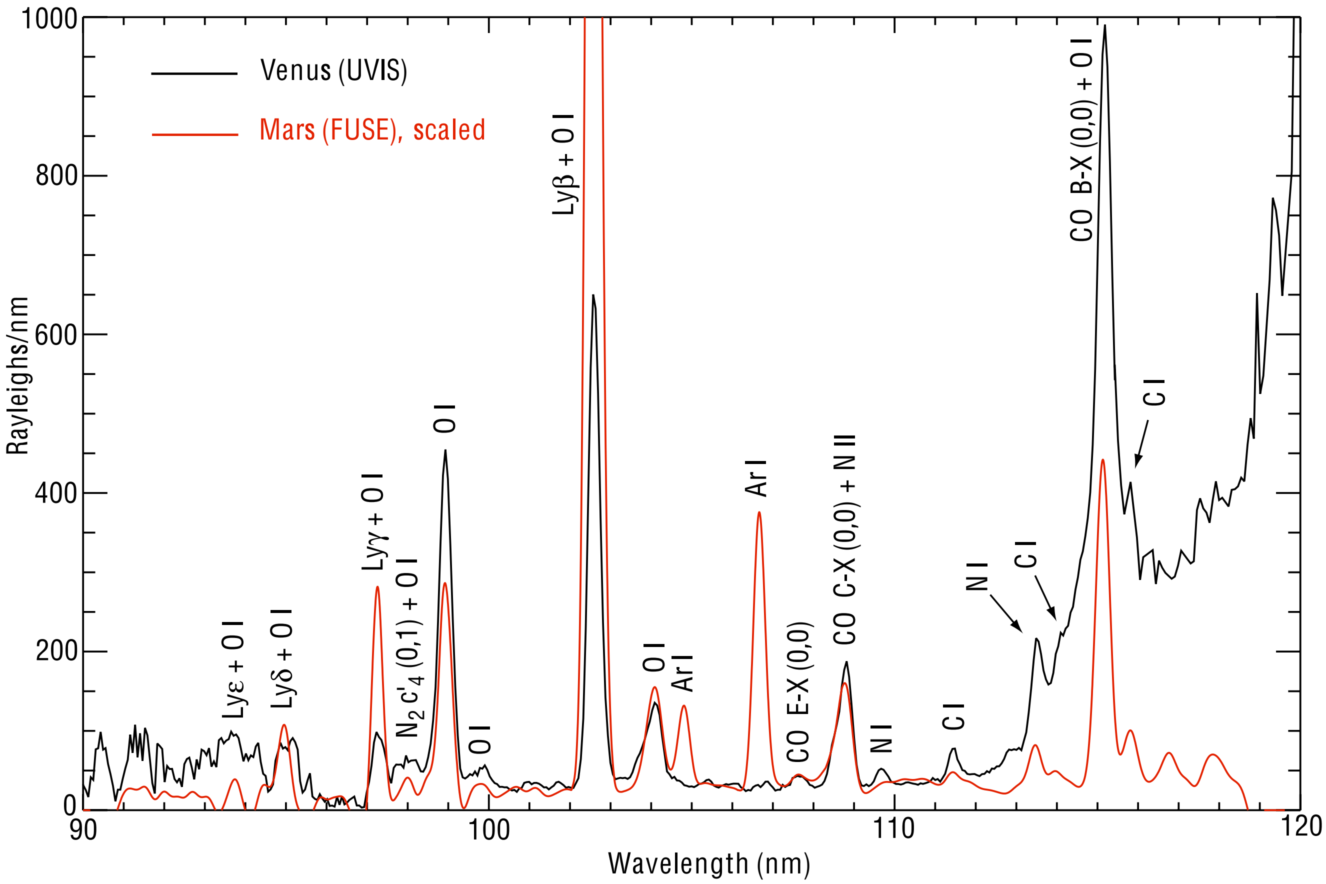

Venus (UVIS)
Mars (FUSE), scaled
Rayleighs/nm
Wavelength (nm)
0
200
400
600
800
1000
90
100
110
120
Lyε + O I
Lyδ + O I
Lyγ + O I
N_2 c'$_4$ (0,1) + O I
O I
O I
Lyβ + O I
O I
Ar I
Ar I
CO E-X (0,0)
CO C-X (0,0) + N II
N I
C I
N I
C I
CO B-X (0,0) + O I
C I

Fig. 2

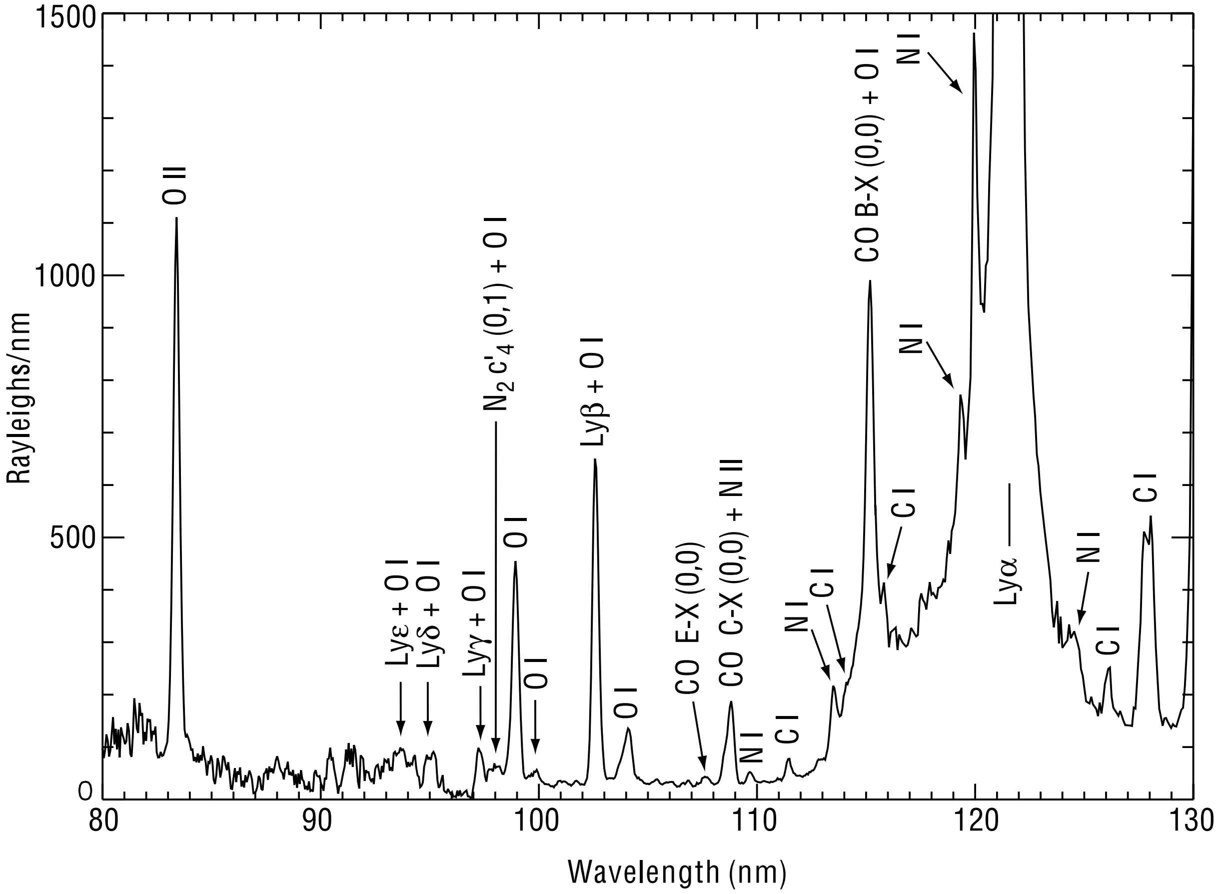
O II
Lyε + O I
Lyδ + O I
Lyγ + O I
N2 c'4 (0,1) + O I
O I
O I
Lyβ + O I
O I
CO E-X (0,0)
CO C-X (0,0) + N II
N I
C I
N I
C I
C I
CO B-X (0,0) + O I
N I
N I
Lyα
N I
C I
C I
Rayleighs/nm
Wavelength (nm)
0
500
1000
1500
80
90
100
110
120
130

Fig. 3

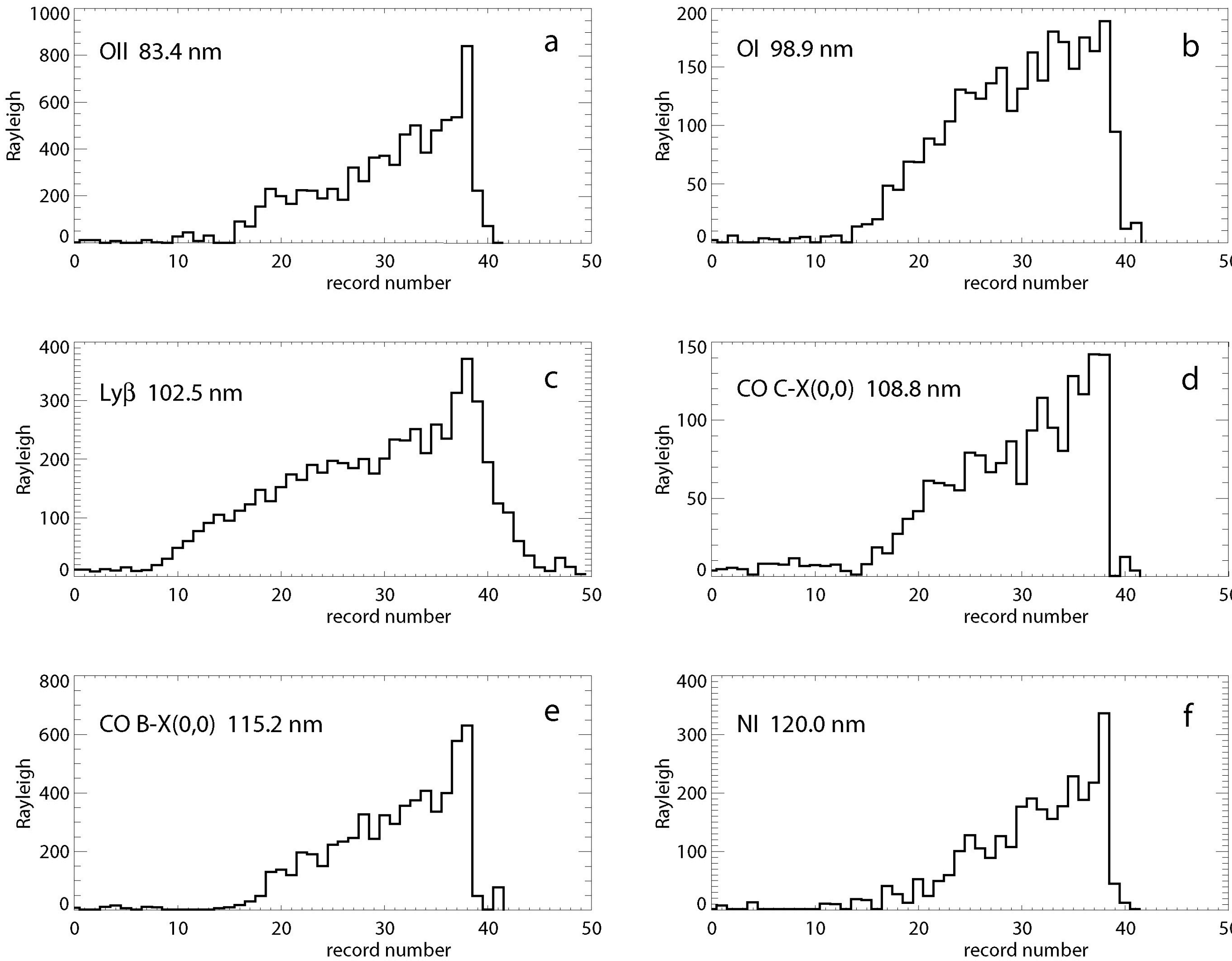
OII 83.4 nm
a
OI 98.9 nm
b
Lyβ 102.5 nm
c
CO C-X(0,0) 108.8 nm
d
CO B-X(0,0) 115.2 nm
e
NI 120.0 nm
f
Rayleigh
record number

Fig. 4

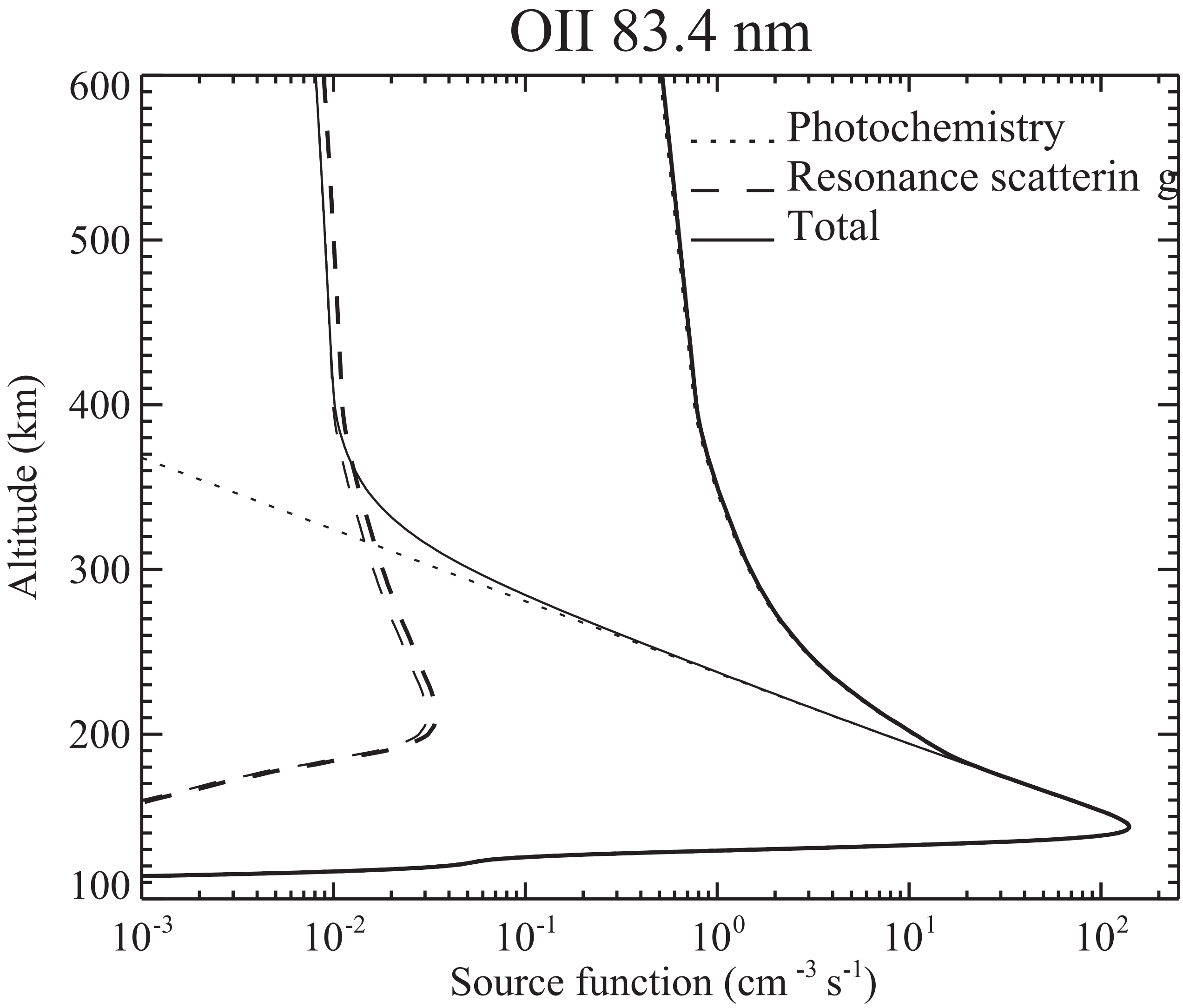
OII 83.4 nm
Photochemistry
Resonance scatterin g
Total
Altitude (km)
100
200
300
400
500
600
10-3
10-2
10-1
100
101
102
Source function (cm -3 s-1)

Fig. 5

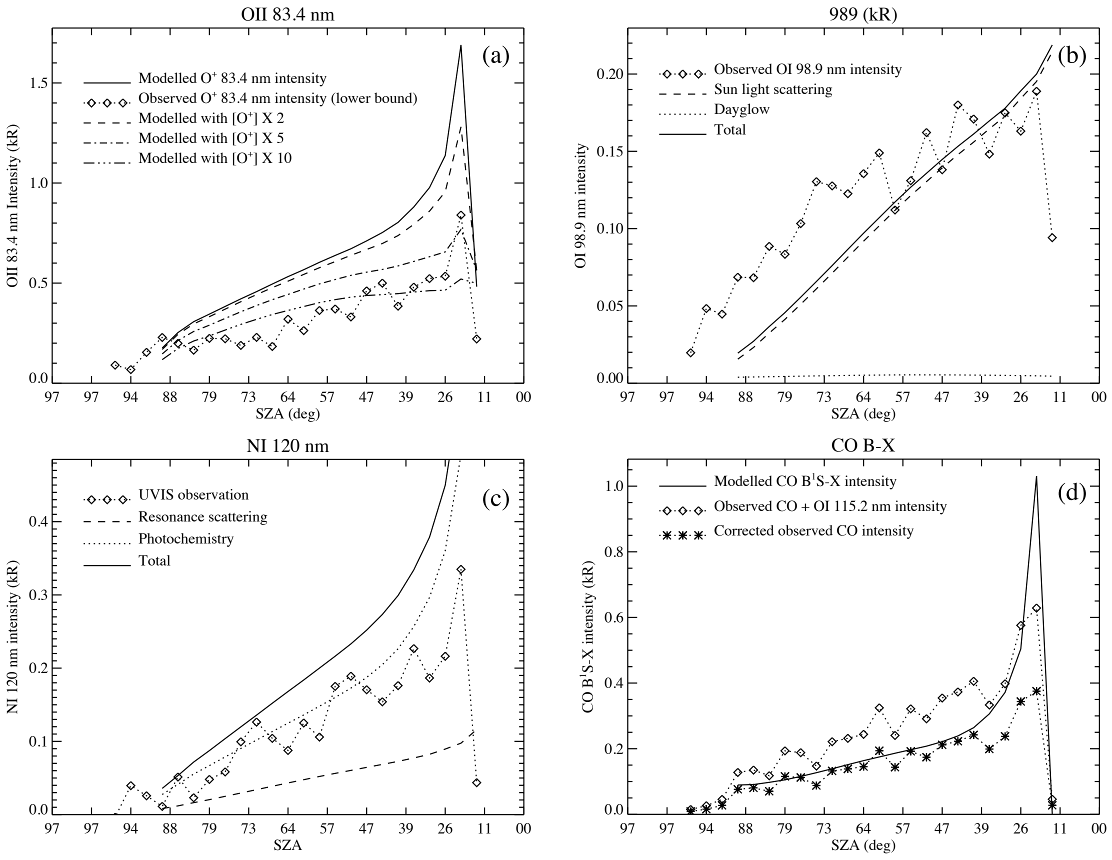
OII 83.4 nm
(a)
Modelled O^{+} 83.4 nm intensity
Observed O^{+} 83.4 nm intensity (lower bound)
Modelled with [O^{+}] X 2
Modelled with [O^{+}] X 5
Modelled with [O^{+}] X 10
OII 83.4 nm Intensity (kR)
SZA (deg)
989 (kR)
(b)
Observed OI 98.9 nm intensity
Sun light scattering
Dayglow
Total
OI 98.9 nm intensity
SZA (deg)
NI 120 nm
(c)
UVIS observation
Resonance scattering
Photochemistry
Total
NI 120 nm intensity (kR)
SZA
CO B-X
(d)
Modelled CO B^{1}S-X intensity
Observed CO + OI 115.2 nm intensity
Corrected observed CO intensity
CO B^{1}S-X intensity (kR)
SZA (deg)

Figure 6

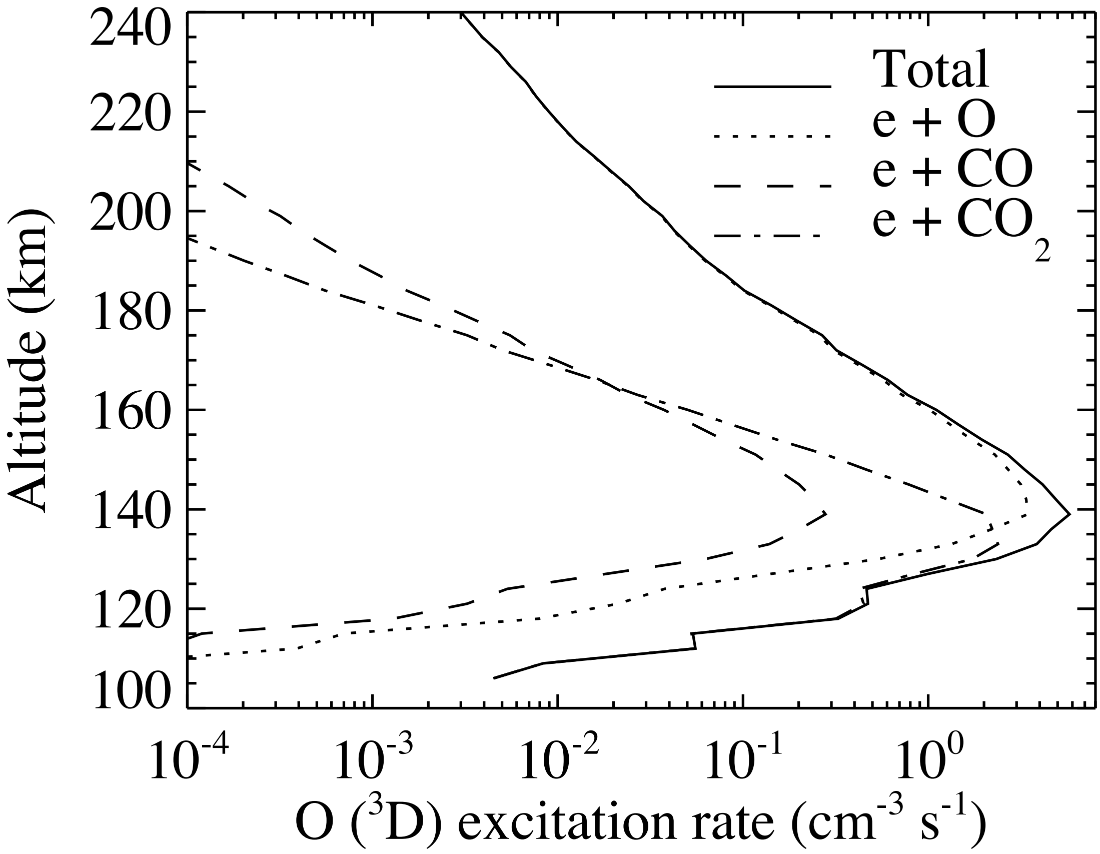
Total
e + O
e + CO
e + CO2
Altitude (km)
240
220
200
180
160
140
120
100
10-4
10-3
10-2
10-1
100
O (3D) excitation rate (cm-3 s-1)

Fig. 7

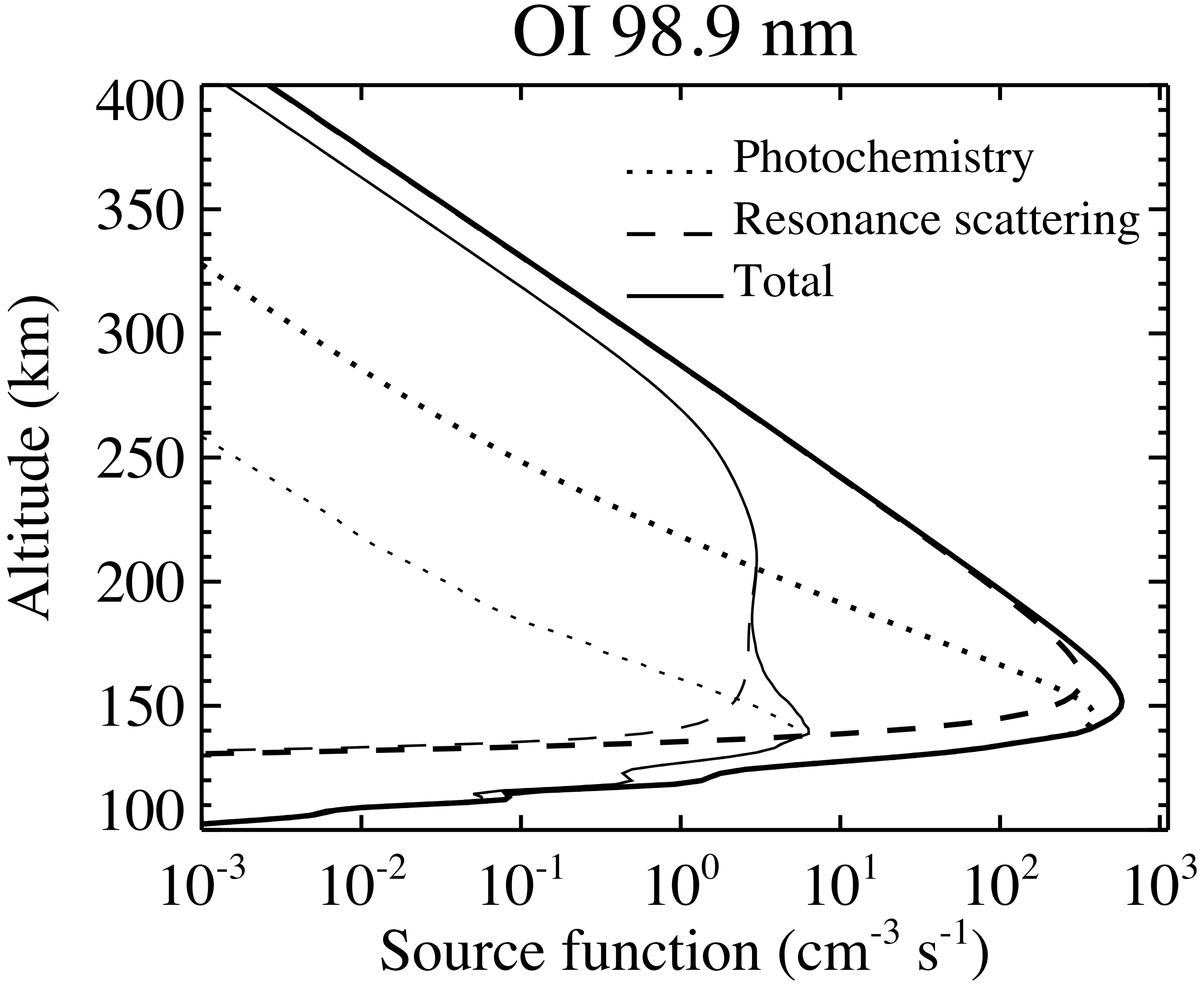
OI 98.9 nm
Photochemistry
Resonance scattering
Total
Altitude (km)
400
350
300
250
200
150
100
10^{-3} 10^{-2} 10^{-1} 10^{0} 10^{1} 10^{2} 10^{3}
Source function (cm^{-3} s^{-1})

Fig. 8

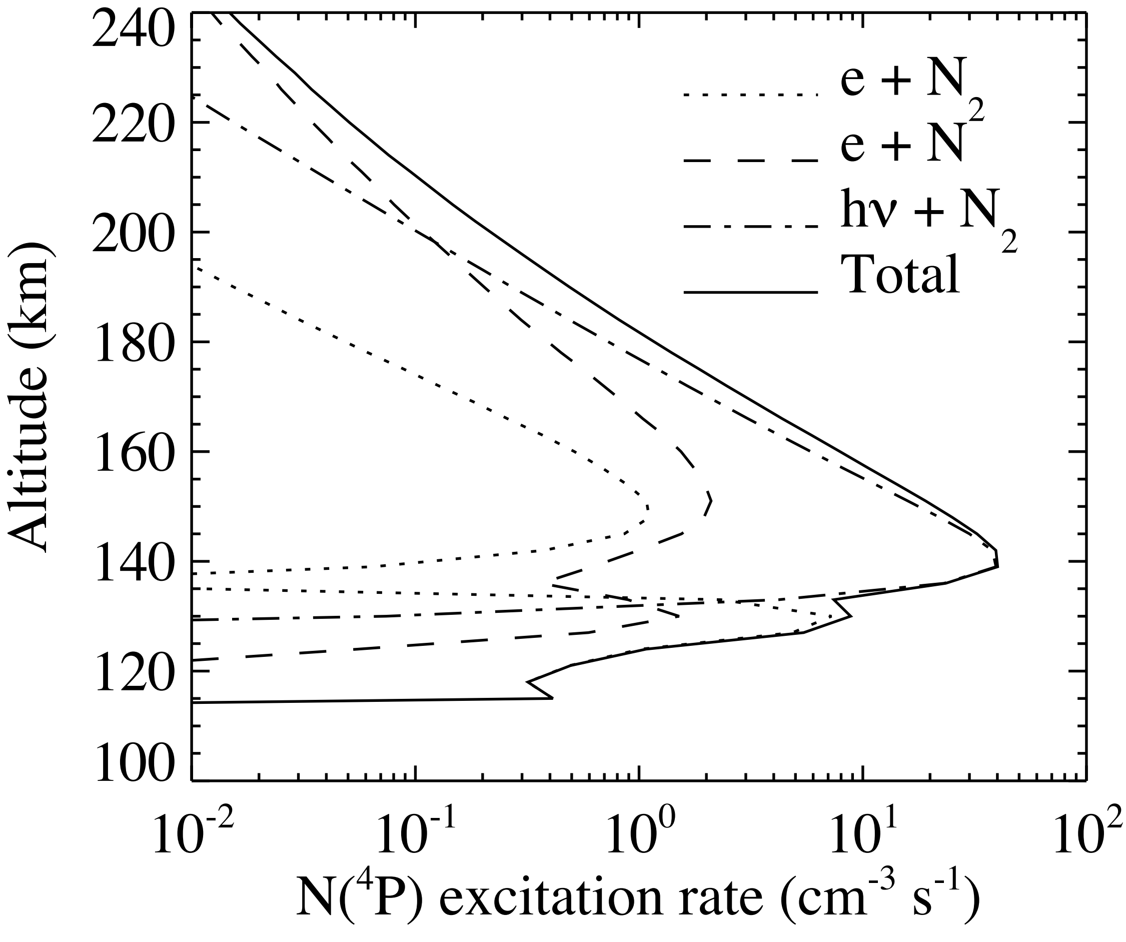

240
220
200
180
160
140
120
100
Altitude (km)
10-2
10-1
100
101
102
N(4P) excitation rate (cm-3 s-1)
e + N2
e + N2
hν + N2
Total

Figure 9

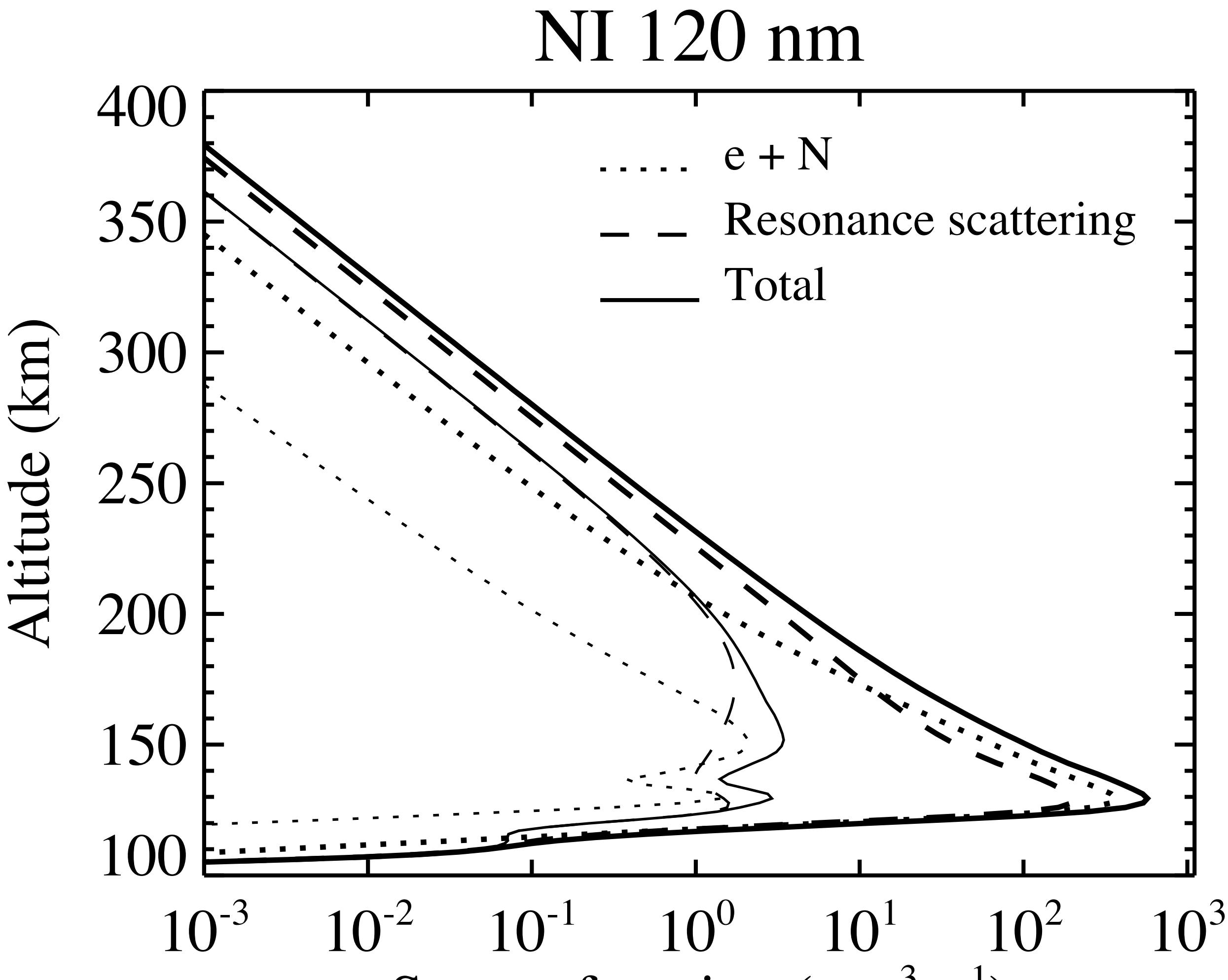
NI 120 nm
e + N
Resonance scattering
Total
Altitude (km)
400
350
300
250
200
150
100
10^-3
10^-2
10^-1
10^0
10^1
10^2
10^3
Source function (cm^-3 s^-1)

Figure 10

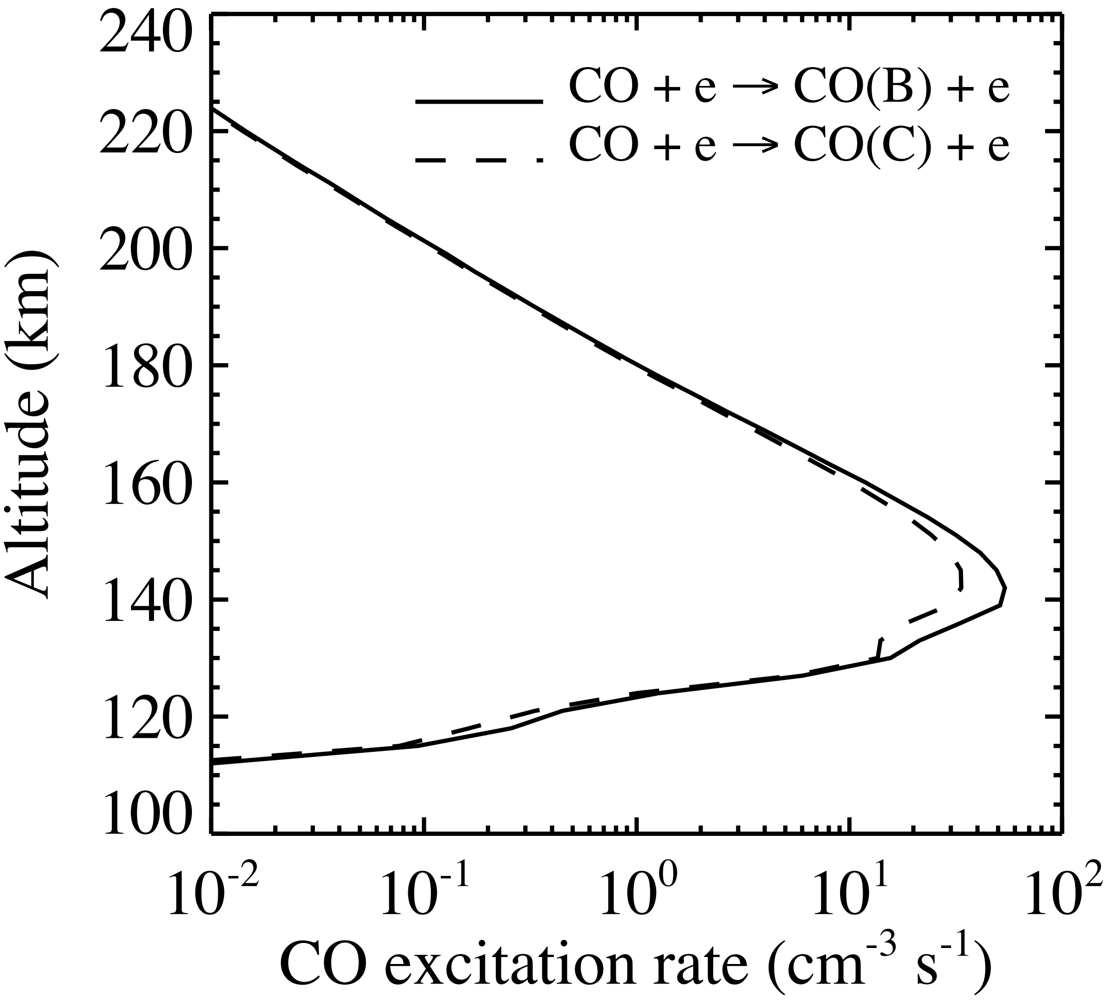
CO + e → CO(B) + e
CO + e → CO(C) + e
Altitude (km)
240
220
200
180
160
140
120
100
10^-2
10^-1
10^0
10^1
10^2
CO excitation rate (cm^-3 s^-1)

Fig. 11